Journal of Biomolecular NMR (2005) 33: 199–211
DOI 10.1007/s10858-005-4425-x

Article

SOFAST-HMQC experiments for recording two-dimensional heteronuclear correlation spectra of proteins within a few seconds

Paul Schanda[a], Ēriks Kupče[b] & Bernhard Brutscher[a,*]
[a]*Institut de Biologie Structurale – Jean-Pierre Ebel, UMR5075 CNRS-CEA-UJF, 41, rue Jules Horowitz, 38027, Grenoble Cedex, France;* [b]*Varian Ltd., Walton-on-Thames, Surrey, KT12 2QF, United Kingdom*

Received 20 June 2005; Accepted 13 October 2005

Key words: Ernst angle, fast NMR, HMQC, longitudinal relaxation enhancement, protein, residual dipolar couplings

Abstract

Fast multidimensional NMR with a time resolution of a few seconds provides a new tool for high throughput screening and site-resolved real-time studies of kinetic molecular processes by NMR. Recently we have demonstrated the feasibility to record protein ^{1}H–^{15}N correlation spectra in a few seconds of acquisition time using a new SOFAST-HMQC experiment (Schanda and Brutscher (2005) *J. Am. Chem. Soc.* **127**, 8014). Here, we investigate in detail the performance of SOFAST-HMQC to record ^{1}H–^{15}N and ^{1}H–^{13}C correlation spectra of proteins of different size and at different magnetic field strengths. Compared to standard ^{1}H–^{15}N correlation experiments SOFAST-HMQC provides a significant gain in sensitivity, especially for fast repetition rates. Guidelines are provided on how to set up SOFAST-HMQC experiments for a given protein sample. In addition, an alternative pulse scheme, IPAP-SOFAST-HMQC is presented that allows application on NMR spectrometers equipped with cryogenic probes, and fast measurement of one-bond ^{1}H–^{13}C and ^{1}H–^{15}N scalar and residual dipolar coupling constants.

Introduction

Multidimensional (nD) heteronuclear NMR provides the required spectral resolution for resolving individual nuclear sites in a macromolecule, by correlating the frequencies of different nuclei and spreading the correlation peaks over several frequency axes. Unfortunately, nD NMR is an intrinsically time-consuming spectroscopic method. Whereas 1D NMR has the multiplex advantage of yielding all frequencies within a single scan, nD NMR relies on the acquisition of multiple scans with stepwise incrementation of an evolution delay for each additional dimension. This not only translates into long acquisition times (several weeks) for the set of NMR spectra necessary to solve the structure of a protein by NMR, it also limits its application for real-time studies of slow dynamic processes in proteins, or its use as a high-throughput screening tool. Therefore, there is an increasing interest in new methods for fast acquisition of multidimensional NMR data.

The time required for the acquisition of an nD NMR spectrum is determined by the sensitivity of the experiment for a given sample and spectrometer, the number of indirectly sampled dimensions (n−1), and the desired spectral resolution. During recent years, continuous efforts in advancing magnet and spectrometer technology have led to a

*To whom correspondence should be addressed.
E-mail: bernhard.brutscher@ibs.fr

significant gain in sensitivity. As the signal to noise (S/N) ratio in the NMR spectrum roughly increases with the square root of the experimental time, these technical improvements translate into a reduction of the acquisition time by up to two orders of magnitude. Therefore, today the time requirement for many NMR experiments is in the *sampling-limited* regime. This means that, even if the S/N ratio is acceptable within a few scans, 2D NMR still demands tens or hundreds of experimental repetitions for linear sampling of the indirect time domain. Consequently, the acquisition time increases exponentially with the number of dimensions. In order to accelerate NMR data acquisition, one has to solve this *data sampling problem* either by limiting the number of sampled data points, or by reducing the time delay between scans required to allow the spin system to relax towards its thermal equilibrium state. Most of the existing fast acquisition techniques are based on the first solution, incomplete sampling of the $n-1$ dimensional time space. Examples are non-uniform data sampling combined with non-linear processing schemes (Hoch and Stern, 2001; Mandelshtam, 2000), reduced dimensionality or projection NMR (Szyperski et al., 1993; Brutscher et al., 1994; Kim and Szyperski, 2003; Kupce and Freeman, 2004), and Hadamard NMR (Kupce et al., 2003; Brutscher, 2004) where data sampling is realized directly in the frequency domain. All these methods basically allow recording of multidimensional correlation spectra in an experimental time ranging from a few minutes up to several hours.

The ultimate solution to the NMR data sampling problem has recently been proposed and experimentally demonstrated by Frydman and co-workers (Frydman et al., 2002). Their ingenious concept of ''single-scan'' NMR allows recording of any multidimensional NMR spectrum within a single repetition of the experiment. Despite the high potential of single-scan NMR for future biomolecular applications, this technique currently requires a very high intrinsic sensitivity and spectrometer hardware optimized for both NMR spectroscopy and imaging purposes. For application to proteins in aqueous solution, several scans are generally required to yield good water suppression and acceptable signal to noise in a few seconds of experimental time.

Recently we have introduced SOFAST-HMQC as an alternative technique for fast acquisition of 2D heteronuclear correlation spectra (Schanda and Brutscher, 2005). Fast data acquisition in SOFAST-HMQC is realized by using very short inter-scan delays. SOFAST-HMQC combines the advantages of a small number of radio-frequency pulses, Ernst-angle excitation (Ernst et al., 1987; Ross et al., 1997), and longitudinal relaxation optimization (Pervushin et al., 2002; Atreya and Szyperski, 2004) to obtain an increased signal to noise ratio for high repetition rates of the experiment. SOFAST-HMQC relies on standard data sampling in the indirect dimension and is therefore easily implemented on any commercially available high-field NMR spectrometer. Here we discuss in detail the performance of different implementations of the SOFAST-HMQC experiment under various experimental conditions, demonstrating the high sensitivity provided by these pulse schemes to record ^{1}H–^{15}N and ^{1}H–^{13}C correlation spectra of proteins at millimolar concentration in a few seconds of experimental time.

SOFAST-HMQC experiments

General features of SOFAST-HMQC

Figure 1a shows the basic pulse scheme to record band-Selective Optimized-Flip-Angle Short-Transient (SOFAST) HMQC spectra. This pulse sequence provides the required high sensitivity to perform fast heteronuclear H–X correlation experiments of macromolecules by using very short recycle delays (t_{rec}). The main features of SOFAST-HMQC are the following: (i) the HMQC-type H–X transfer steps require only few rf pulses which limits signal loss due to B_1-field inhomogeneities and pulse imperfections. A reduced number of rf pulses will be especially important if the experiment is performed on a cryogenic probe, where B_1-field inhomogeneities are more pronounced. (ii) The band-selective ^{1}H pulses reduce the effective spin-lattice relaxation times (T_1) of the observed ^{1}H spins. The presence of a large number of non-perturbed ^{1}H spins, interacting with the observed ^{1}H via dipolar interactions (NOE effect), significantly reduces longitudinal relaxation times whereby the equilibrium spin polarization is more quickly restored. This effect has previously been described and observed for protein

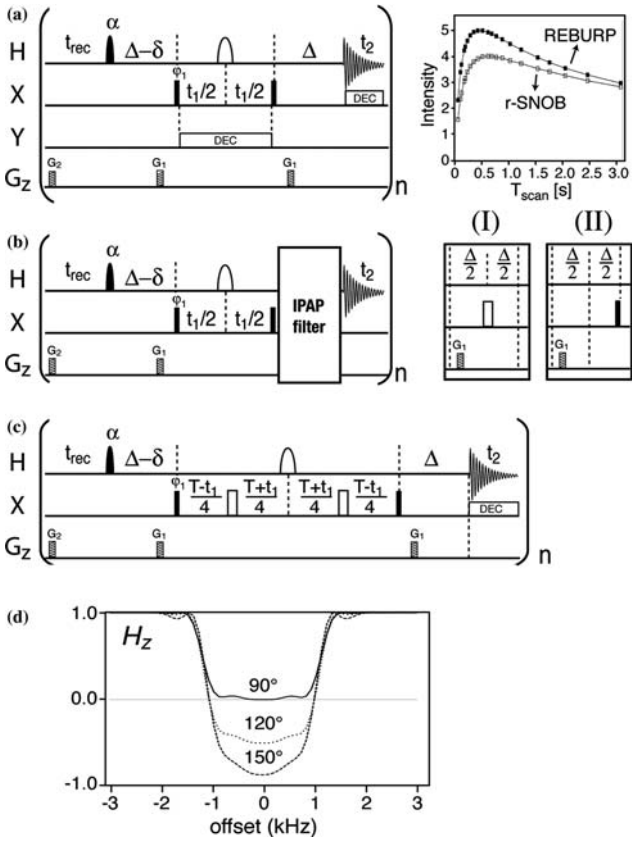

Figure 1. Pulse sequences to record SOFAST-HMQC ^{1}H–X (X = ^{13}C or ^{15}N) correlation spectra: (a) basic pulse scheme, (b) IPAP version, and (c) CT version. Filled and open pulse symbols indicate 90° and 180° rf pulses, except for the ^{1}H excitation pulse applied with flip angle α. The variable-flip-angle pulse has a polychromatic PC9 shape (Kupce and Freeman, 1994), and band-selective ^{1}H refocusing is realized using either REBURP (Geen and Freeman, 1991) or r-SNOB (Kupce et al., 1995). The transfer delay Δ is set to $1/(2J_{HX})$, and t_{rec} is the recycle delay between scans. The delay δ accounts for spin evolution during the PC9 pulse, and has to be adjusted prior to data acquisition to yield pure-phase spectra in the ^{1}H dimension. The CT delay T in (c) is set to $T = n/J_{XX}$ with n an integer. To avoid extensive first order phase corrections in the t_1 dimension of experiments (a) and (b), for t_1 delays shorter than the REBURP pulse length the 90°–t_1–90° pulse sequence element on the ^{15}N channel is applied simultaneously to the REBURP pulse on the ^{1}H channel. Quadrature detection in t_1 is obtained by phase incrementation of φ_1 according to STATES or TPPI-STATES. In standard SOFAST-HMQC (a) adiabatic WURST-2 decoupling (Kupce and Wagner, 1995) is applied on X during detection. For IPAP-SOFAST-HMQC two experiments are recorded as indicated in the inserts of (b). In experiment (I), ^{1}H–X coupling evolution during Δ is refocused by application of a 180° X pulse. In experiment (II),^{1}H–X coupling evolution is active during Δ. The 90° X pulse applied before final detection converts any remaining antiphase coherence of the type $2H_xX_z$ into undetectable multiple quantum coherence. This purge pulse is mainly useful for the measurement of H–X coupling constants of partially aligned protein samples. The two data sets (I) and (II) are then added or subtracted prior to Fourier transformation to yield the upfield or downfield components of the ^{1}H doublet line, respectively. Note that IPAP filtering can also be applied in the CT-SOFAST-HMQC sequence shown in (c) by simply omitting the X decoupling during detection, and replacing the back-transfer delay Δ by the two inserts shown in (b). The graph in the upper right corner shows a comparison of the performance of REBURP (upper curve) and r-SNOB (lower curve) when used in the SOFAST-HMQC sequence (a) to record ^{1}H–^{15}N correlation spectra. The data were recorded at 600 MHz ^{1}H frequency on a sample of ^{15}N-labeled ubiquitin using a flip angle $\alpha = 90°$ and pulse lengths of 3.0, 2.03, and 0.77 ms for the PC9, REBURP, and r-SNOB pulses, respectively. In (d) simulated excitation profiles of PC9 are plotted as a function of frequency offset for flip angles $\alpha = 90°, 120°$, and 150°. The calculation has been performed for 600 MHz ^{1}H frequency and a pulse length of 3.0 ms. The SOFAST-HMQC experiments, presented here, have been implemented in the Varian Bio-pack. The pulse sequence code for Bruker and Varian spectrometers, and pulse shape files are also available from the authors upon request.

samples by Pervushin and co-workers (Pervushin et al., 2002). As will be shown later on, the longitudinal relaxation optimization enhancement effect depends on the number and type of the applied ^{1}H pulses. The use of only 2 (band-selective) ^{1}H pulses in SOFAST-HMQC ensures minimal perturbation

of the undetected proton spins, and provides higher enhancement factors than observed with other longitudinal relaxation optimized pulse schemes (Pervushin et al., 2002). As long as the water resonance is outside the selected ^{1}H pulse bandwidth, the WATERGATE-type (Piotto et al., 1992) pulse sequence element G_1–180°(^{1}H)–G_1 yields efficient water suppression within a single scan. The selective ^{1}H manipulation also removes coupling evolution between excited ^{1}H spins and passive ^{1}H spins from frequency bands that are not perturbed by the selective pulses. A disadvantage of the band-selective spin manipulation is that only ^{1}H–X spin systems resonating inside the chosen band width are detected in the final spectrum. (iii) The adjustable flip angle of the ^{1}H excitation pulse allows further enhancement of the available steady-state magnetization for a given recycle delay. Ernst and coworkers (Ernst et al., 1987) have shown that maximal signal is obtained for the so-called Ernst angle β_{opt} given by

$$\beta_{opt} = \cos^{-1}(\exp(-T_{rec}/T_1)) \quad (1)$$

with T_{rec} the effective ^{1}H longitudinal relaxation delay including the interscan delay (t_{rec}), the acquisition times $t_1/2$ and t_2, and the transfer delay Δ. T_1 is the effective spin-lattice relaxation time constant assuming mono-exponential polarization recovery. The signal to noise ratio (S/N) of SOFAST-HMQC per unit experimental time, neglecting transverse spin relaxation effects and other sources of signal loss, is then given by

$$S/N \propto \frac{(1-\exp(-T_{rec}/T_1))\sin\beta}{1-\exp(-T_{rec}/T_1)\cos\beta}\frac{1}{\sqrt{nT_{Scan}}} \quad (2)$$

with β the effective flip angle $\beta = \alpha - 180°$ taking into account the effect of the ^{1}H refocusing pulse, and T_{scan} the time required for a single scan including the pulse sequence duration, acquisition time, and the inter-scan delay (t_{rec}).

Band-selective ^{1}H pulses in SOFAST-HMQC

The performance of SOFAST-HMQC critically depends on the choice of the pulse shapes for the band-selective excitation and refocusing pulses on the ^{1}H channel. We have initially chosen a r-SNOB profile (Kupce et al., 1995) for refocusing which presents the advantage of a short pulse length thus reducing signal loss due to transverse spin relaxation (Schanda and Brutscher, 2005). In the meanwhile, we have tested other pulse shapes and have found that, for the recording of ^{1}H–^{15}N correlation spectra, a REBURP profile yields higher sensitivity despite a 3-times longer pulse duration. An experimental comparison of r-SNOB and REBURP performance in ^{1}H–^{15}N SOFAST-HMQC is shown in Figure 1a. A signal increase of up to 50% is observed when using REBURP instead of r-SNOB for short scan times. This surprising result can be explained by the better off-resonance performance of REBURP, resulting in less perturbation of the aliphatic ^{1}H spin polarization and, as a consequence, shorter longitudinal relaxation times of the amide proton spins. This is manifest by the maximum of the intensity curves, shifted towards shorter scan times for the experiments realized using REBURP. A similar behavior was also observed for other proteins varying in size and different magnetic field strengths (data not shown).

In order to implement the feature of optimized flip-angle band-selective excitation in the SOFAST-HMQC we have explored the literature for suitable pulse shapes. Most of the band-selective "top-hat" pulse shapes commonly used for NMR spectroscopy, e.g. BURP (Geen and Freeman, 1991), Gaussian pulse cascades (Emsley and Bodenhausen, 1992), or SNOB (Kupce et al., 1995), have only been optimized for discrete flip angles of 90° or 180°, and generally are not useful for variable flip angle excitation purposes. In contrast, polychromatic (PC) selective pulses have been shown to perform well for a whole range of flip angles (Kupce and Freeman, 1994). These PC pulses are based on a series of simultaneously applied, frequency shifted basic pulse elements. For the present applications we have used the PC9 pulse shape, which has the desired "top-hat" excitation profile for flip angles $0° < \alpha < 120°$. For the flip-angles of 120° to 150° used in this work, the excitation profile slightly deteriorates (Figure 1d), but the combination of PC9 and REBURP (or r-SNOB) pulses still yields good experimental results. For even larger flip-angles the excitation profile of PC9 deteriorates significantly, resulting in large variations of the effective flip angles over the excitation band width. Unlike other band-selective excitation pulses that yield "pure-phase" transverse magnetization, the PC9 pulses produce phase that is a linear function of the frequency offset. Schematically, one can thus

replace a PC9 pulse by the combination of a pure-phase excitation pulse followed by a delay δ. The chemical shift and scalar J_{HX} coupling evolution occurring during this delay δ can be accounted for by adjusting the subsequent transfer delay of the HMQC sequence to $1/(2J_{HX}) - \delta$ (see Figure 1). If the delay δ has been properly adjusted prior to data acquisition no first-order phase correction is required in the ^{1}H dimension. Otherwise, pure-phase spectra can still be obtained by applying a first order phase correction.

IPAP-SOFAST-HMQC and CT-SOFAST-HMQC

Alternatives to the basic SOFAST-HMQC pulse scheme are shown in Figure 1b and c. In IPAP-SOFAST-HMQC (Figure 1b) the heteronuclear X decoupling during acquisition (t_2) is replaced by an IPAP filter (Ottiger et al., 1998; Andersson et al., 1998). The IPAP filter is realized by the two sequence blocks shown in the inserts of Figure 1b. Two spectra have to be recorded with and without refocusing of the^{1}H–X coupling evolution during the back-transfer delay Δ, thus increasing the minimal experimental time by a factor of 2. Addition or subtraction of these spectra then separates the two ^{1}H doublet components in different sub-spectra. Each of the 2 sub-spectra has a 2-times lower S/N ratio than a standard SOFAST-HMQC spectrum recorded in the same experimental time (corresponding to the acquisition of both sub spectra). A single correlation spectrum is obtained by adding the 2 sub-spectra after appropriate shifting of the two spectra with respect to each other in the ^{1}H dimension by an amount of $\pm(J_{HX})/2$. This results in a √2 increase in S/N ratio, and consequently the sensitivity (S/N per unit experimental time) of IPAP-SOFAST-HMQC is decreased by a factor √2 with respect to the standard SOFAST-HMQC pulse scheme of Figure 1a. For larger molecules and high magnetic field strengths cross-correlated relaxation effects induce differential broadening of the ^{1}H doublet lines in the absence of ^{15}N decoupling. Adding the 2 lines, a broad and a narrow one, will result in complicated (non-Lorentzian) line shapes in the ^{1}H dimension, but also increases the sensitivity of IPAP-SOFAST-HMQC (TROSY effect). The main interest of the IPAP-version of SOFAST-HMQC is that it does not require composite X decoupling during detection. Reducing rf power becomes an important issue when applying the SOFAST-HMQC experiment on NMR spectrometers equipped with a cryogenic probe. In this case the √2-sensitivity loss due to the IPAP filtering is largely compensated by the 2 to 4-times higher sensitivity provided by the probe. IPAP-SOFAST-HMQC also offers the possibility of fast measurement of heteronuclear H–X (scalar or residual dipolar) spin–spin coupling constants yielding useful additional probes of structural changes occurring during kinetic processes that can be monitored by real-time NMR.

SOFAST-HMQC can also be combined with constant time (CT) frequency editing in the indirect dimension (t_1). The pulse sequence for CT-SOFAST-HMQC is shown in Figure 1c. This CT version is mainly useful for removing line splittings due to ^{13}C–^{13}C couplings in ^{1}H–^{13}C correlation experiments, thus providing increased spectral resolution at the expense of sensitivity. The experiment can be either implemented with heteronuclear decoupling during detection or an IPAP filter for application on cryogenic probes, or measurement of ^{1}H–X spin coupling constants.

Application to proteins

^{1}H–^{15}N SOFAST-HMQC

The SOFAST-HMQC pulse sequences of Figure 1 have been designed to provide high sensitivity for fast repetition rates. To examine the performance of the SOFAST-HMQC experiment for the desired short interscan delays we have measured 1D spectra of ^{15}N-labeled ubiquitin and of ^{13}C,^{15}N-labeled SiR-FP18, the flavodoxin-like domain of the *E. coli* sulfate reductase. Figure 2 shows the measured S/N ratios for constant experimental time as a function of the duration of a single repetition of the experiment T_{scan} (taking into account the length of the pulse sequence, data acquisition time, and recycle delay) for ubiquitin (Figure 2a and b) and for SiR-FP18 (Figure 2c and d). Each intensity point was obtained by scaling all spectra to the same noise level according to the number of applied scans, and integrating the spectral intensity over the range 7.0–9.5 ppm. The curves are therefore representative of the average behavior of the experiment for all amide sites in

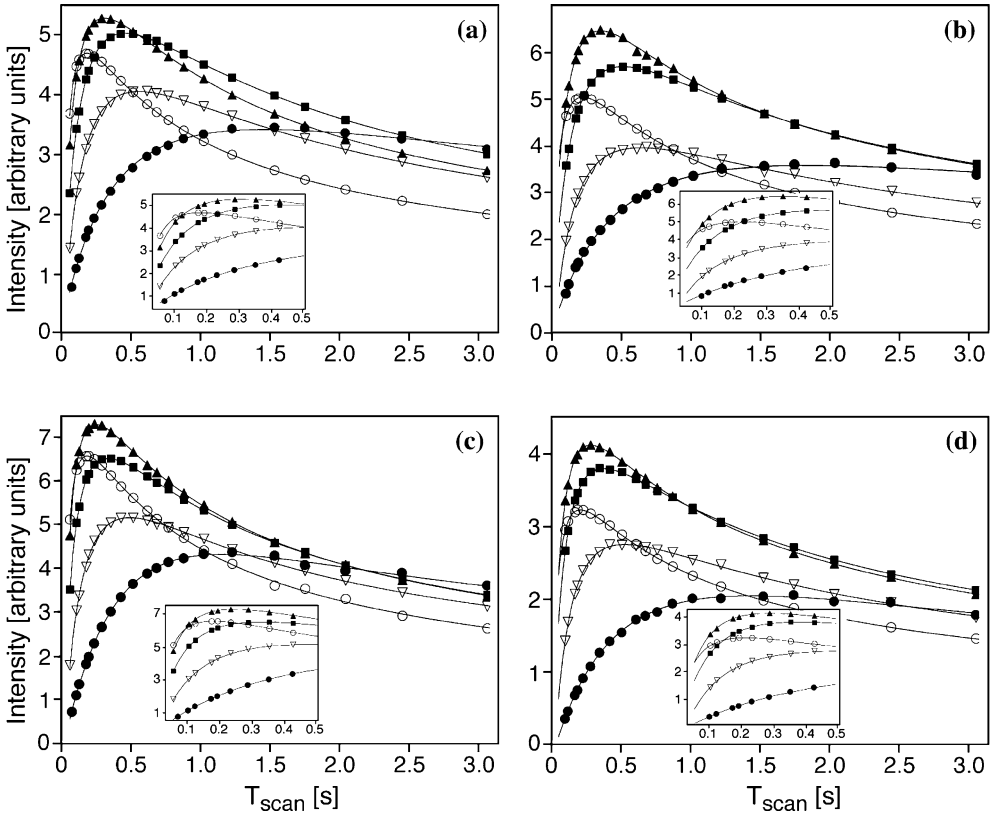

Figure 2. Signal-to-noise ratios per unit time (intensity) plotted as a function of the scan time (T_{scan}) obtained with different ^{1}H–^{15}N correlation experiments for (a) ubiquitin (8.6 kDa, 2 mM, 25 °C, pH 6.2) at 600 MHz, (b) ubiquitin at 800 MHz, (c) SiR-FP18 (18 kDa, 1.8 mM, 25 °C, pH 7.0) at 600 MHz, and (d) SiR-FP18 at 800 MHz. The 800 MHz spectrometer was equipped with a cryogenic probe, whereas the experiments at 600 MHz ^{1}H frequency were performed on a standard (non cryogenic) probe. The intensities were extracted from 1D spectra recorded using the SOFAST-HMQC sequence of Figure 1a ($t_1 = 0$) with flip angles of $\alpha = 90°$ (squares), 120° (triangles) and 150° (open circles), LHSQC (open triangles), and se-wfb HSQC (filled circles). Band-selective ^{1}H pulses in the SOFAST-HMQC and LHSQC experiments were centered at 8.0 ppm covering a bandwidth of 4.0 ppm. Variable flip angle excitation and refocusing in SOFAST-HMQC were realized using a PC9 pulse of 3.0 ms and a REBURP pulse of 2.03 ms, respectively. The se-wfb-HSQC experiments were recorded using the pulse sequence implemented in the Varian Bio-pack. The LHSQC sequence was set up as described by Pervushin et al. (2002), except for the final INEPT delays τ_2 and τ_3 that were reduced to 1.0 ms to account for spin evolution during the REBURP pulse. The inserts show an expansion of the data for short scan times. Each spectrum was acquired in the same experimental time, and the spectra were scaled to the same noise level. The se-wfb-HSQC spectra were scaled up by a factor $\sqrt{2}$ to account for the gain in S/N ratio obtained by the sensitivity-enhanced quadrature detection in the 2D version of the experiment. Intensities were obtained by integration of the 1D ^{1}H spectra over the spectral range 7.0–9.5 ppm. The solid lines are smoothened interpolations of the experimental data points.

the protein. The SOFAST-HMQC data for three different flip angles (90°, 120°, and 150°) are compared to results from a sensitivity-enhanced (se) water-flipback (wfb) HSQC pulse sequence as implemented in the Varian Bio-pack, and from a longitudinal relaxation optimized HSQC (LHSQC) experiment (Pervushin et al., 2002). The peak intensities in the se-wfb-HSQC spectra were up-scaled by a factor of $\sqrt{2}$ to account for the sensitivity-enhanced quadrature detection providing a $\sqrt{2}$-signal enhancement in the 2D version of the experiment with respect to standard quadrature detection as implemented in SOFAST-HMQC and LHSQC. Theoretically we expect that the different quadrature detection schemes translate into a sensitivity advantage of $\sqrt{2}$ for se-wfb-HSQC with respect to SOFAST-HMQC and LHSQC at long recycle delays. In practice, we find that this sensitivity difference is partly or completely compensated by the larger number of pulses applied in se-wfb-HSQC leading to increased signal losses due to pulse imperfections and B_1-field inhomogeneities. As expected, this effect is more pronounced for the data acquired using a

cryogenic probe (Figure 2b and d), characterized by larger B_1-field gradients across the detection volume. For shorter scan times the reduced effective spin-lattice ^1H relaxation times become important, resulting in a higher sensitivity for the longitudinal-relaxation optimized pulse sequences (SOFAST-HMQC and LHSQC). The more efficient spin-lattice relaxation is reflected in the shift of the maximum of the intensity curves (T_{scan}^{opt}) towards shorter scan times. This shift is more pronounced for SOFAST-HMQC than for LHSQC. This observation is most likely explained by the larger number of ^1H pulses required for LHSQC, resulting in some perturbation of the aliphatic and water ^1H equilibrium spin polarization. Using the relation $T_{\text{scan}}^{\text{opt}} = 1.25 * T_1$ (see Equation [2]) one can estimate average effective ^1H spin-lattice relaxation times of $T_1 \approx 0.9$–1.4 s for HSQC, of $T_1 \approx 0.4$–0.5 s for LHSQC, and of $T_1 \approx 0.3$–0.4 s for SOFAST-HMQC ($\alpha = 90°$). For all experiments, we observe an increase in the average effective T_1 times with increasing B_0 field strength and with decreasing molecular weight (or tumbling correlation time) of the molecule. For very short scan times the sensitivity advantage of SOFAST-HMQC with respect to se-wfb HSQC and LHSQC becomes even more pronounced when using larger flip angles $\alpha > 90°$. As shown in the inserts of Figure 2a–d important signal enhancements are observed for $T_{\text{scan}} < 200$ ms when using SOFAST-HMQC instead of se-wfb HSQC or LHSQC. This sensitivity enhancement allows significantly reduced experimental times for a given S/N ratio.

The 1D spectra in Figure 2 provide only information on the average signal to noise ratio obtained by the different pulse sequences. In order to look in more detail at the spread of peak intensities among the amide protons in SOFAST-HMQC, we have recorded a 2D ^1H–^{15}N correlation map of ubiquitin at 600 MHz ^1H frequency using a short scan time of $T_{\text{scan}} = 165$ ms and an optimized flip angle $\alpha = 120°$ (see Figure 2a). This spectrum, shown in Figure 3a can be compared to spectra recorded using se-wfb-HSQC (Figure 3d), LHSQC (Figure 3b), and sensitivity-enhanced aliphatic-flip-back HSQC (se-afb-HSQC) pulse sequences (Figure 3c). For se-afb-HSQC the water-flip-back pulse in the standard se-wfb-HSQC sequence has been replaced by a band-selective EBURP flip-back pulse. Although, for this scan time all longitudinal-relaxation optimized experiments provide a significant gain in signal to noise ratio with respect to the standard se-wfb-HSQC experiment, SOFAST-HMQC is by far the most sensitive. A residue-by-residue analysis of the peak intensities measured in the different 2D spectra of Figure 3 shows a sensitivity gain for SOFAST-HMQC with respect to se-wfb-HSQC varying between 2 and 6, whereas this gain is only about 1.5 to 3.5 for LHSQC, and even less for se-afb-HSQC despite its $\sqrt{2}$-sensitivity advantage provided by the sensitivity-enhanced quadrature detection scheme. This sensitivity advantage of SOFAST-HMQC with respect to se-wfb-HSQC is slightly reduced when using longer t_1 acquisition times, e.g. $t_1^{\max} = 50$ ms (open circles) instead of $t_1^{\max} = 28$ ms (filled circles), because of the shorter transverse relaxation times of ^1H–^{15}N multiple quantum (MQ) coherence in HMQC-type sequences with respect to ^{15}N single-quantum (SQ) coherence evolution in HSQC-type sequences. The variations in the measured intensity ratio along the protein backbone are indicative of differences in the local proton density at the individual amide sites and/or differences in local dynamics.

The principal conclusions from these experimental results are the following: (i) If optimized acquisition parameters (scan time, flip angle) are used, and moderate t_1 acquisition times are acceptable, SOFAST-HMQC yields the most sensitive ^1H–^{15}N correlation spectra of folded proteins. (ii) In the context of very fast data acquisition, SOFAST-HMQC provides a much higher sensitivity than se-wfb-HSQC using the same scan times, and a similar sensitivity as se-wfb-HSQC recorded with optimized inter-scan delays. The intensity curves shown in Figure 2 also provide some guidelines for setting up SOFAST-HMQC experiments. The highest sensitivity is obtained for scan times between 200 and 300 ms using a flip angle of $\alpha = 120°$, independent of the molecular size or magnetic field strength, whereas for shorter scan times ($T_{\text{scan}} < 200$ ms) flip angles of $\alpha = 130°$–$150°$ are advantageous. For practical applications it is recommended to fix the scan time (recycle delay) and then optimize the flip angle of the PC9 excitation pulse experimentally by recording a series of 1D SOFAST-HMQC spectra varying the power level (flip angle) of the PC9 pulse.

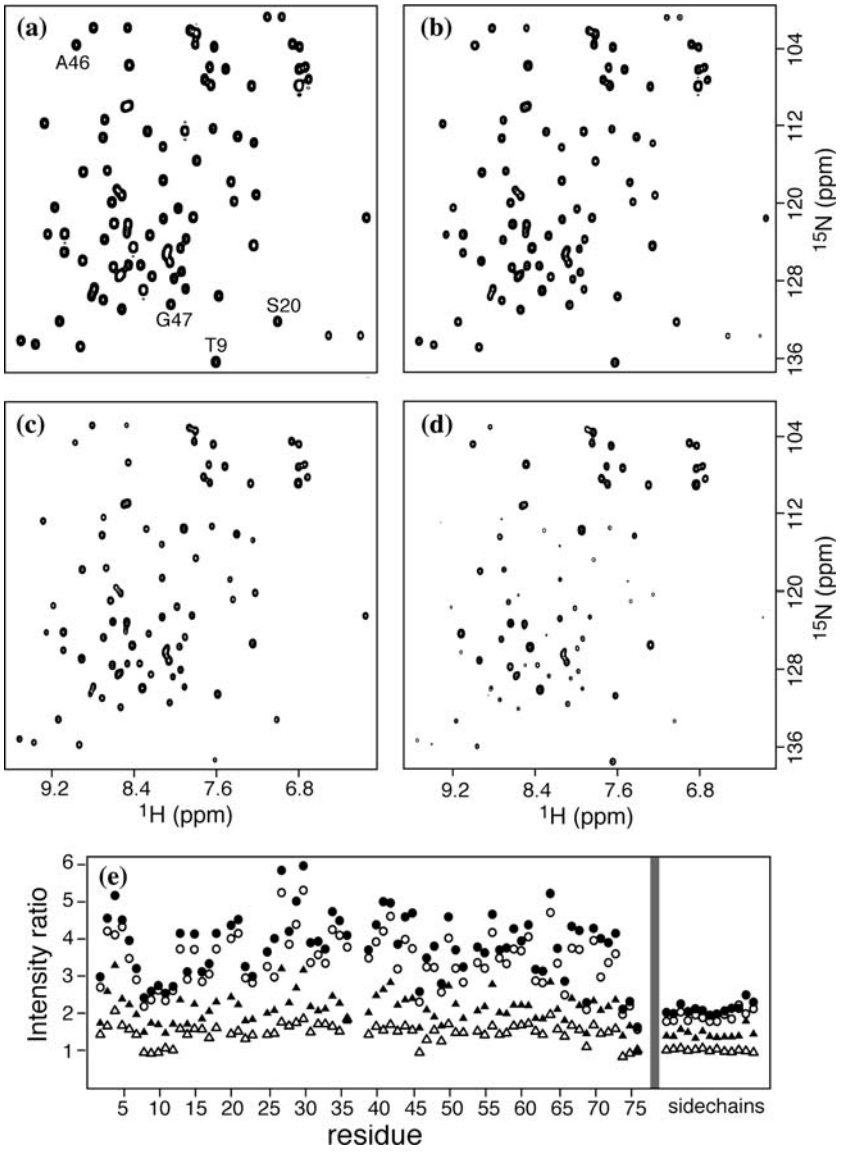

Figure 3. Comparison of 2D ^{1}H–^{15}N correlation spectra of ubiquitin recorded at 600 MHz using (a) the SOFAST-HMQC pulse sequence of Figure 1a ($\alpha = 120°$), (b) the LHSQC sequence of Pervushin et al. (2002), (c) a longitudinal-relaxation optimized se-afb-HSQC sequence and (d) a standard se-wfb-HSQC sequence as provided by the Varian Bio-pack. For se-afb-HSQC, the water-flip-back pulse in the standard se-wfb-HSQC sequence was replaced by a band-selective EBURP flip-back pulse covering the ^{1}H frequency range from −1 to 5 ppm. ^{1}H excitation and refocusing in SOFAST-HMQC were realized using a PC9 pulse of 3.0 ms and a REBURP pulse of 2.03 ms, respectively. All spectra were acquired with a scan time of $T_{scan} = 165$ ms, and the acquisition times were set to $t_1^{max} = 28$ ms, and $t_2^{max} = 40$ ms. ^{15}N-decoupling during t_2 was realized using WURST-2 (Kupce and Wagner, 1995) at an average field strength of $\gamma B_1/2\pi = 550$Hz. Additional 2D spectra were recorded with a longer t_1 acquisition time of $t_1^{max} = 50$ ms (not shown). In (e) intensity ratios are plotted as a function of the peptide sequence: SOFAST-HMQC over se-wfb-HSQC for $t_1^{max} = 28$ ms (filled circles) and $t_1^{max} = 50$ ms (open circles), LHSQC over se-wfb-HSQC (filled triangles), and se-afb-HSQC over se-wfb-HSQC (open triangles).

SOFAST-HMQC using cryogenic probes

The use of a cryogenic probe is very attractive in the context of fast data acquisition as cryogenic probes provide the required high sensitivity to record protein correlation spectra in a short overall experimental time. Unfortunately, the rf power necessary for the standard SOFAST-HMQC pulse

sequence (Figure 1a) at high magnetic field using short inter-scan delays often exceeds the allowed duty cycle of currently available cryogenic probes. We therefore propose an alternative sequence where the X-decoupling is replaced by an IPAP filter. This IPAP-SOFAST-HMQC sequence, shown in Figure 1b, has allowed us to record a ^{1}H–^{15}N correlation spectrum on a ^{15}N-labelled sample of ubiquitin at submillimolar concentration on a 800 MHz spectrometer equipped with a cryogenic probe. The spectrum recorded in an overall experimental time of 12 s is shown in Figure 4. Data acquisition details are provided in the figure caption. The high S/N ratio obtained in this short experimental time is highlighted by the 1D trace extracted along the ^{15}N dimension, demonstrating the performance of the IPAP-SOFAST-HMQC for application on high-field NMR spectrometers equipped with cryogenic probes.

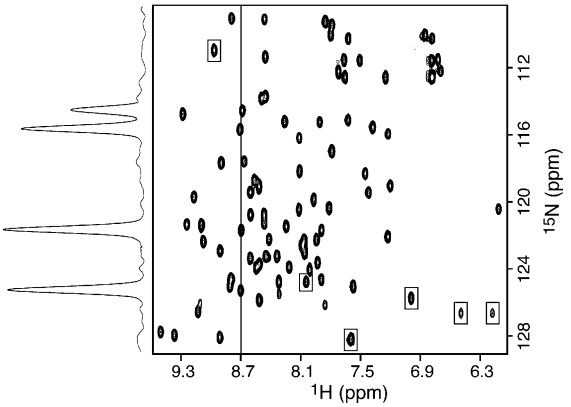

Figure 4. ^{1}H–^{15}N correlation spectrum of ^{15}N-labeled ubiquitin (0.9 mM, 25 °C, pH 6.2) recorded on an 800 MHz INOVA spectrometer equipped with a cryogenic probe using the IPAP-SOFAST-HMQC sequence of Figure 1b. The band-selective ^{1}H excitation (PC9) and refocusing (REBURP) pulses were centered at 8.0 ppm covering a bandwidth of 4.0 ppm, resulting in pulse lengths of 2.25 and 1.52 ms, respectively. The acquisition parameters were set to $\alpha = 140°, \Delta = 5.4$ ms, $\delta = 1.2$ ms, $t_1^{max} = 22$ ms, $t_2^{max} = 40$ ms, and $t_{rec} = 1.0$ ms. Forty complex data points were acquired in the t_1 dimension and four additional scans without data acquisition to reach a steady state ($n = 80 + 4$). Two data sets were recorded as explained in the caption to Figure 1b, in an overall experimental time of 12 s. For data processing, the two raw data sets were first added and subtracted yielding the new data sets S1 and S2. Then a first order phase shift $\Delta\varphi_1 = +(2\pi SWJ_{HN})/2$ and $\Delta\varphi_1 = -(2\pi SWJ_{HN})/2$ was applied in the t_2 dimension to S1 and S2, respectively, with SW the spectral width in the ^{1}H dimension. Finally the two data sets were added and Fourier transformed as usual. Boxes indicate cross peaks with a ^{15}N frequency outside the chosen ^{15}N spectral width of 1800 Hz that are folded back into the spectrum.

Fast measurement of ^{1}H–^{15}N coupling constants

A second interest of the IPAP-SOFAST-HMQC sequence is that it allows fast measurement of H–X (^{1}H–^{15}N or ^{1}H–^{13}C) spin coupling constants from the ^{1}H frequency difference of cross peaks detected in the two sub-spectra corresponding to the α and β spin states of the attached hetero-nuclei. The quantification of one-bond spin coupling constants is especially interesting in the presence of an alignment medium that induces a dipolar contribution to the line splitting (Tjandra and Bax, 1997). These residual dipolar couplings provide valuable information about molecular structure and dynamics (Blackledge, 2005).

For fully protonated, partially aligned protein samples, one-bond (scalar and residual dipolar) spin coupling constants can be accurately measured from the line splitting observed along the heteronuclear frequency dimension in spin-state-selective H–X correlation experiments. In IPAP-SOFAST-HMQC the couplings are measured in the directly detected ^{1}H dimension, which is intrinsically less accurate. The ^{1}H line shape for aligned protein samples is generally asymmetric because of the presence of numerous ^{1}H–^{1}H dipolar interactions inducing a fine structure in the peak shape, and cross-correlated relaxation effects responsible for unequal line widths and intensities of the individual multiplet lines (Brutscher, 2000). This induces some systematic error in the coupling measurements. In order to evaluate experimentally the performance of IPAP-SOFAST-HMQC, in terms of accuracy and precision for the measurement of ^{1}H–^{15}N (scalar and residual dipolar) coupling constants, we have performed an IPAP-SOFAST-HMQC experiment on a partially aligned 2 mM sample of ^{15}N-labeled ubiquitin, dissolved in aqueous solution containing a 5% C12E5/hexanol mixture ($r = 0.85$) (Ruckert and Otting, 2000). The quadrupolar ^{2}H line splitting observed for these conditions was about 30 Hz at 30 °C. The IPAP-SOFAST-HMQC sub-spectra, corresponding to the down- and upfield ^{1}H doublet components, are shown in Figure 5a and b. A total of 58 coupling constants could be quantified from non-overlapping cross peaks in these spectra, obtained in an overall experimental time of only 12 s. These results can be compared to couplings

measured along the ^{15}N dimension of TROSY-type spin-state selective ^{1}H–^{15}N correlation spectra (Weigelt, 1998) recorded in an experimental time of 25 min. The correlation of the two data sets, shown in Figure 5c, is quite good, although a systematic error (as mentioned above) tends to slightly underestimate the couplings measured using the fast IPAP-SOFAST-HMQC approach. In conclusion, IPAP-SOFAST-HMQC is certainly not the best method for precise and accurate measurement of ^{1}H–^{15}N residual dipolar couplings for NMR structure determination, but the quality of the data, nevertheless, demonstrates the potential of SOFAST-HMQC for probing structural changes in proteins that occur on a time scale of seconds via the fast measurement of one-bond spin couplings in partially aligned protein samples.

^{1}H–^{13}C SOFAST-HMQC of methyl groups

The SOFAST-HMQC experiment is not limited to ^{1}H–^{15}N correlation spectroscopy, but can also be used to record ^{1}H–^{13}C correlation spectra of sub-ensembles of aliphatic and aromatic protons in the protein. As an attractive first example we demonstrate here its application to methyl groups. Methyl groups are valuable probes of structure and dynamics as they are dispersed throughout the primary sequence and often located in the hydrophobic core of proteins. Due to the rapid rotation, methyl groups possess three equivalent protons, which intrinsically yields a threefold intensity improvement. Their location in the hydrophobic core should make them excellent probes for following folding reactions, where the hydrophobic core is formed starting from a highly solvent-exposed structural ensemble. It has also been shown that methyl groups are useful probes for the study of molecular interfaces, and drug binding (Hajduk et al., 2000). Thus there is an interest in methods that allow recording very fast ^{1}H–^{13}C methyl correlation spectra.

The relatively good spectral separation of methyl ^{1}H resonances (−0.5 to 1.5 ppm) from other aliphatic proton resonances makes the extension of SOFAST-HMQC to this spin system straightforward. Figure 6a and b show ^{1}H–^{13}C methyl correlation spectra of SiR-FP18 and ubiquitin, respectively, recorded with the pulse sequence of Figure 1a. The spectra were recorded on standard triple-resonance (non cryogenic) probes in an overall experimental time of 16 s

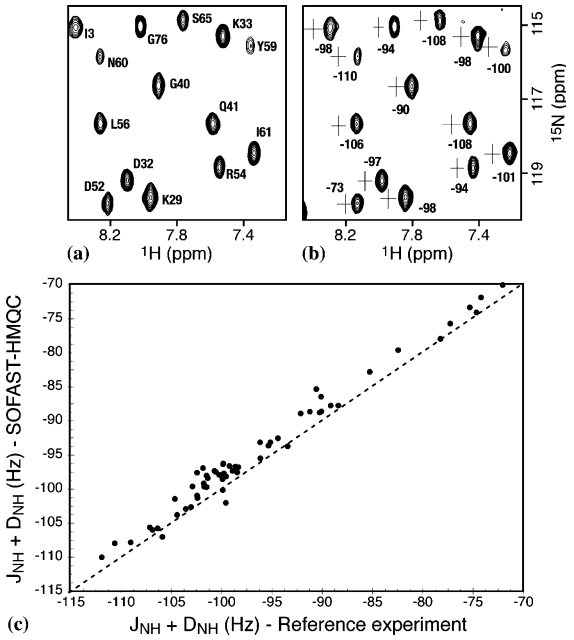

Figure 5. Experimental demonstration of fast ^{1}H–^{15}N coupling measurement using SOFAST-HMQC. Spectra were recorded at a 800 MHz spectrometer equipped with a cryogenic probe on a 2 mM sample of ubiquitin aligned in an alcohol mixture (Ruckert and Otting, 2000) at 30 °C. Two data sets were acquired using the IPAP-version of SOFAST-HMQC as explained in the caption to Figure 1b. A small part of the two sub-spectra containing the downfield and upfield doublet components are shown in (a) and (b), respectively. A cross in (b) indicates the position of the corresponding doublet peak in spectrum (a). In addition, residue number and type information is given in (a), and the measured coupling constants (in Hz) are provided in (b). The same acquisition parameters were used as reported for the spectrum of Figure 4 yielding an overall experimental time of 12 s. In (c) the measured coupling constants are plotted against the line splittings measured in the ^{15}N dimension from a pair of TROSY-type ^{1}H–^{15}N spin-state selective correlation spectra (Weigelt, 1998) recorded in an experimental time of 25 min.

(Figure 6a) and 10 s (Figure 6b). Contrary to amide ^{1}H–^{15}N SOFAST-HMQC, for methyl spectra the use of an r-SNOB pulse shape for ^{1}H refocusing yielded better results than the use of a REBURP pulse. This finding already indicates that the longitudinal relaxation enhancement effect is less pronounced for methyl protons than for amide protons. Further experimental details are given in the figure caption. Methyl correlation spectra of proteins often suffer from severe signal overlap. To increase spectral resolution, additional homonuclear ^{13}C decoupling (Y channel in Figure 1a) was applied during t_1 as described in

detail previously (Van Melckebeke et al., 2004). This homo-decoupling removes J_{CC} line splittings in the ^{13}C dimension except for methyls at the δ position of isoleucine and leucine residues and therefore also yields a gain in sensitivity. An alternative to homonuclear decoupling is the use of CT ^{13}C editing, allowing increased spectral resolution in the ^{13}C dimension at the expense of sensitivity. Because of the relatively long transverse relaxation times of ^{1}H–^{13}C MQ coherences in methyl groups, CT editing only slightly reduces the sensitivity of the experiment for small proteins such as ubiquitin. A ^{1}H–^{13}C CT-SOFAST-HMQC recorded using the pulse sequence of Figure 1c in an experimental time of 10 s is shown in Figure 6c. 1D traces extracted along the ^{13}C dimension highlight the sensitivity and spectral resolution obtained by the SOFAST-HMQC experiments. Methyl proton spin-lattice relaxation is dominated by the dipolar interaction among the methyl ^{1}H and ^{13}C that is time modulated by the fast methyl rotation, and only to a smaller extent by interactions with non-methyl protons in the surrounding. Therefore the longitudinal ^{1}H relaxation enhancement using selective methyl ^{1}H manipulation in SOFAST-HMQC is minor, yielding only a slight signal enhancement with respect to a standard HSQC experiment. This is demonstrated in Figure 7 showing the average S/N ratio of the methyl cross peaks as a function of the scan time. Much larger effects are expected for other more rigid aliphatic or aromatic ^{1}H sites in the protein. Still, for short inter-scan delays the optimized flip angle in SOFAST-HMQC provides on average a 50% signal increase with respect to standard HSQC.

SOFAST-HMQC may also prove useful for application to large molecular systems with a high level of deuteration and specific ^{1}H and ^{13}C labels at the methyl positions. (Rosen et al., 1996), where the MQ coherence evolution yields TROSY-type line narrowing (Tugarinov et al., 2003), and the optimized flip angle provides increased sensitivity for short inter-scan delays.

Conclusions

SOFAST-HMQC provides a robust new tool for biomolecular NMR. It allows adjusting the acquisition time of two-dimensional heteronuclear

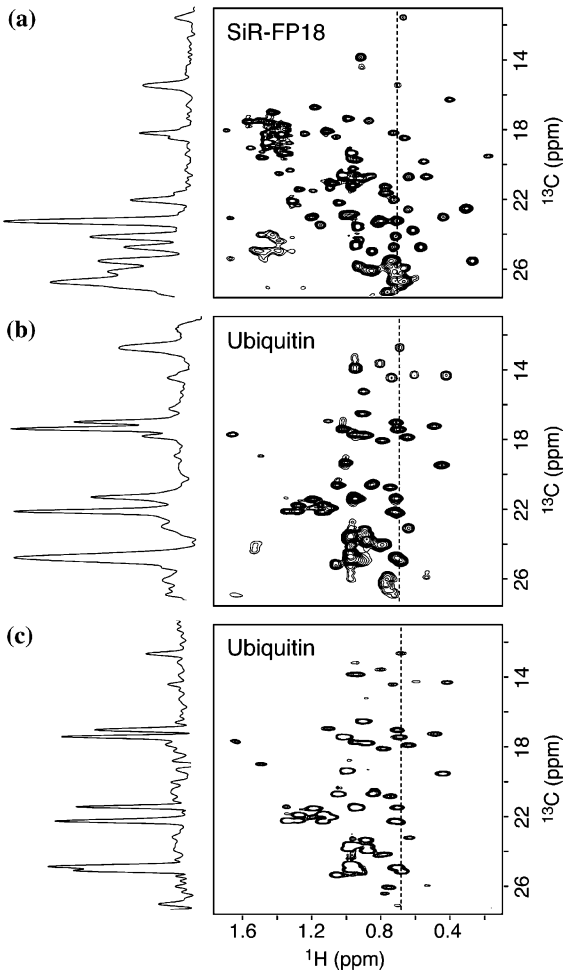

Figure 6. Methyl ^{1}H–^{13}C SOFAST-HMQC spectra of (a) SiR-FP18 (1.5 mM, 30 °C, 800 MHz), (b) ubiquitin (2 mM, 25 °C, 600 MHz), both recorded using the pulse sequence of Figure 1a, and (c) ubiquitin (2 mM, 25 °C, 600 MHz) using the CT-SOFAST-HMQC sequence of Figure 1c. The band-selective ^{1}H excitation (PC9) and refocusing (r-SNOB) pulses were centered at 0.7 ppm covering a bandwidth of 2.0 ppm, resulting in pulse length of 4.5 and 1.15 ms, respectively. The acquisition parameters at 800 MHz were set to $\alpha = 150°, \Delta = 3.8$ ms, $\delta = 2.5$ ms, $t_1^{max} = 30$ ms, $t_2^{max} = 40$ ms, and $t_{rec} = 1.0$ ms. 120 complex data points were acquired in t_1, $n = 240 + 4$ dummy scans, yielding a total experimental time of 16 s for the spectrum in (a). At 600 MHz the following parameters were used: $\alpha = 150°, \Delta = 3.8$ ms, $\delta = 3.4$ ms, $t_1^{max} = 30$ ms (23 ms), $t_2^{max} = 40$ ms, and $t_{rec} = 1.0$ ms. 80 (60) complex data points were acquired in t_1, $n = 160$ (120) + 4 dummy scans, yielding a total experimental time of 10 s for the spectra in (b) and (c). The values in parenthesis correspond to the settings of the CT experiment shown in (c). Multiple-band selective ^{13}C decoupling during methyl ^{13}C frequency editing was realized by a train of CA-WURST-2 (Kupce and Freeman, 1996) pulses of lengths $\tau_p = 5$ ms, centered at 37, 53, and 70 ppm, and covering bandwidths of 12 ppm each (Van Melckebeke et al., 2004).

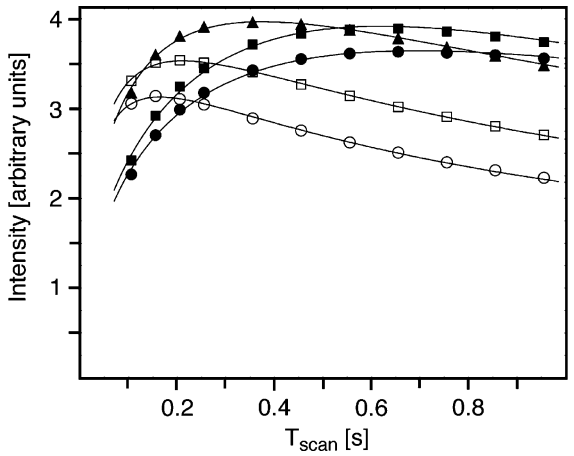

Figure 7. Signal-to-noise ratios per unit time (intensity) plotted as a function of the scan time (T_{scan}) obtained with different ^{1}H–^{13}C methyl correlation experiments for ubiquitin (2 mM, 25 °C) at 600 MHz. 2D spectra were recorded using the SOFAST-HMQC sequence of Figure 1a with flip angles of $\alpha = 90°$ (filled squares), 120° (triangles), 140° (open squares) and 150° (open circles), and using a standard HSQC sequence (filled circles). Acquisition parameters are identical to those used for the spectrum in Figure 6b except that no homonuclear ^{13}C decoupling was applied during t_1. The plotted data points correspond to the sum of the intensities measured for 27 well-resolved methyl cross peaks in the 2D spectra.

correlation spectra of proteins as a function of the available sensitivity down to a minimal time of a few seconds. It also provides higher signal to noise ratio for a given experimental time than other ^{1}H–^{15}N correlation experiments. Different implementations of SOFAST-HMQC have been presented, that are optimized for the use on standard or cryogenic NMR probes, for additional homonuclear decoupling in the indirect frequency dimension, and for the measurement of (scalar and residual dipolar) spin coupling constants. In view of the continuously increasing sensitivity of biomolecular NMR instruments, it can be expected that SOFAST-HMQC will become a widespread tool for high-throughput and real-time NMR investigations of protein structure, dynamics, and kinetics.

Acknowledgements

This work was supported by the Commissariat à l'Energie Atomique and the Centre National de la Recherche Scientifique. P.S. acknowledges support from the French ministry of education, research, and technology, and from the Austrian federal ministry of education, science, and culture. We thank Beate Bersch, Isabel Ayala, and Jacques Covès (IBS Grenoble) for the preparation of the isotope-labeled protein samples used in this study, and S. Grzesiek and M. Rogowski (Biozentrum Basel) for kindly providing the ubiquitin expression vector.

References

Andersson, P., Weigelt, J. and Otting, G. (1998) *J. Biomol. NMR*, **12**, 435–441.
Atreya, H.S. and Szyperski, T. (2004) *Proc. Natl. Acad. Sci. USA*, **101**, 9642–9647.
Blackledge, M. (2005) *Prog. Nucl. Magn. Reson. Spectrosc.*, **46**, 23–61.
Brutscher, B. (2000) *Concept. Magnetic Res.*, **12**, 207–229.
Brutscher, B. (2004) *J. Biomol. NMR*, **29**, 57–64.
Brutscher, B., Simorre, J.P., Caffrey, M.S. and Marion, D. (1994) *J. Magn. Reson. B*, **105**, 77–82.
Emsley, L. and Bodenhausen, G. (1992) *J. Magn. Reson.*, **97**, 135–148.
Ernst, R., Bodenhausen, G. and Wokaun, G. (1987) *Principles of Nuclear Magnetic Resonance in One and Two Dimensions*, Oxford University Press, Oxford.
Frydman, L., Scherf, T. and Lupulescu, A. (2002) *Proc. Natl. Acad. Sci. USA*, **99**, 15858–15862.
Geen, H. and Freeman, R. (1991) *J. Magn. Reson.*, **93**, 93–141.
Hajduk, P.J., Augeri, D.J., Mack, J., Mendoza, R., Yang, J.G., Betz, S.F. and Fesik, S.W. (2000) *J. Am. Chem. Soc.*, **122**, 7898–7904.
Hoch, J.C. and Stern, A.S. (2001) *Nucl. Mag. Reson. Biol. Macromol., Pt A*, **338**, 159–178.
Kim, S. and Szyperski, T. (2003) *J. Am. Chem. Soc.*, **125**, 1385–1393.
Kupče, E., Boyd, J. and Campbell, I.D. (1995) *J. Magn. Reson. B*, **106**, 300–303.
Kupče, E. and Freeman, R. (1994) *J. Magn. Reson. A*, **108**, 268–273.
Kupče, E. and Freeman, R. (1996) *J. Magn. Reson. A*, **118**, 299–303.
Kupče, E. and Freeman, R. (2004) *J. Am. Chem. Soc.*, **126**, 6429–6440.
Kupče, E., Nishida, T. and Freeman, R. (2003) *Prog. Nucl. Magn. Reson. Spectrosc.*, **42**, 95–122.
Kupče, E. and Wagner, G. (1995) *J. Magn. Reson. B*, **109**, 329–333.
Mandelshtam, V.A. (2000) *J. Magn. Reson.*, **144**, 343–356.
Ottiger, M., Delaglio, F. and Bax, A. (1998) *J. Magn. Reson.*, **131**, 373–378.
Pervushin, K., Vogeli, B. and Eletsky, A. (2002) *J. Am. Chem. Soc.*, **124**, 12898–12902.
Piotto, M., Saudek, V. and Sklenar, V. (1992) *J. Biomol. NMR*, **2**, 661–665.
Rosen, M.K., Gardner, K.H., Willis, R.C., Parris, W.E., Pawson, T. and Kay, L.E. (1996) *J. Mol. Biol.*, **263**, 627–636.
Ross, A., Salzmann, M. and Senn, H. (1997) *J. Biomol. NMR*, **10**, 389–396.

Ruckert, M. and Otting, G. (2000) *J. Am. Chem. Soc.*, **122**, 7793–7797.
Schanda, P. and Brutscher, B. (2005) *J. Am. Chem. Soc.*, **127**, 8014–8015.
Szyperski, T., Wider, G., Bushweller, J.H. and Wuthrich, K. (1993) *J. Am. Chem. Soc.*, **115**, 9307–9308.
Tjandra, N. and Bax, A. (1997) *Science*, **278**, 1111–1114.
Tugarinov, V., Hwang, P.M., Ollerenshaw, J.E. and Kay, L.E. (2003) *J. Am. Chem. Soc.*, **125**, 10420–10428.
Van Melckebeke, H., Simorre, J.P. and Brutscher, B. (2004) *J. Am. Chem. Soc.*, **126**, 9584–9591.
Weigelt, J. (1998) *J. Am. Chem. Soc.*, **120**, 10778–10779.